Solar RRL
www.solar-rrl.com

Record Photocurrent Density over 26 mA cm^{-2} in Planar Perovskite Solar Cells Enabled by Antireflective Cascaded Electron Transport Layer

Xin Luo, Yuan Gao, Pengchen Zhu, Qiaolei Han, Renxing Lin, Han Gao, Yurui Wang, Jia Zhu, Songlin Li, and Hairen Tan**

Planar perovskite solar cells (PSCs) hold promise for simple processing at low temperatures; however, they usually show lower short-circuit current density (J_{sc}) than their mesoporous counterparts owing to their higher primary optical reflection losses at the front side. The antireflective nature of a mesoporous electron transport layer (ETL) enables a low optical reflection in the front surface of solar cells, which is challenging to realize in planar PSCs. Herein, an antireflective cascaded ETL structure using SnO_2/TiO_2–Cl bilayers is devised to reduce optical reflection losses and to improve electrical performance in planar PSCs. The antireflective cascaded ETL results in an enhanced J_{sc} of 25.4 mA cm^{-2} in formamidinium lead triiodide based planar PSCs, compared with the control J_{sc} of 24.6 mA cm^{-2} using single-layered SnO_2 ETL. A record-high J_{sc} of 26.1 mA cm^{-2} is further achieved using an additional antireflective coating on the front glass side, leading to a power conversion efficiency of 22.9%.

The power conversion efficiency (PCE) of perovskite solar cells (PSCs) has increased from 3.8% to 25.2% over the past decade.[1–7] Two architectures, mesoporous and planar device structures, are commonly used for PSCs. In formal (n-i-p) mesoporous PSCs, a mesoporous electron transport layer (ETL) is used as a scaffold; this mesoporous ETL naturally leads to lower optical reflection in PSCs than planar ETL,[8–11] though requiring high temperature and complex processing. The planar n-i-p structure, in contrast, is simpler to fabricate at low temperatures;[12–15] however, the planar structure usually results in a lower short-circuit current density (J_{sc}) due to higher optical reflection losses at the front side compared with the mesoporous counterparts.[16–18]

Lead halide PSCs with J_{sc} values above 25 mA cm^{-2} are mostly achieved by mesoporous structures using formamidinium lead triiodide ($FAPbI_3$)-based perovskites with a minimal content of methylammonium (MA) and/or bromide.[6,19–21] These mesoporous PSCs have demonstrated the highest certified PCEs, with values above 24% (the highest PCE is 23.7% for planar PSCs).[5,6] Among $FAPbI_3$-based PSCs with bandgaps around 1.50 eV, the highest J_{sc} values (>26 mA cm^{-2}) reported to date were obtained using mesoporous titanium-oxide-based ETL and by introducing MACl or $MDACl_2$ to stabilize α-$FAPbI_3$.[6,21] Their external quantum efficiency (EQE) curves showed an almost flat and uniform absorption higher than 90% in the visible spectral range (400–750 nm), giving a J_{sc} as high as 26.7 mA cm^{-2} (certified, with antireflective coating on glass).[6]

For planar PSCs, You and co-workers achieved the highest certified PCE of 23.7% using SnO_2 nanocrystals (NCs) film as the ETL (≈30 nm thick), where the J_{sc} is 25.2 mA cm^{-2} (with antireflective coating on glass) and the $FAPbI_3$-based perovskite (bandgap ≈1.53 eV) was fabricated using a two-step sequential deposition method.[5,22,23] Efficient planar $FAPbI_3$-based PSCs reported by other groups typically exhibited J_{sc} values in the range of 23.0–24.5 mA cm^{-2}.[24–26] The planar PSCs fabricated by one-step antisolvent method usually showed slightly lower J_{sc} than those processed by two-step method due to the thinner perovskite layers obtained by one-step method.[12,27,28]

The fact that J_{sc} achievable in mesoporous PSCs is higher than that in planar counterparts is attributed to the antireflective effect of the pores in the mesoporous structure. Antireflective strategies such as texturing perovskite films[29–32] and nanostructuring transport layers[33–35] have been attempted to further improve the J_{sc} of planar PSCs. However, the texturing structures result in difficulties for follow-up fabrication steps and consequently degrade the electrical performance of solar cells. We reasoned that the PCE of planar PSCs could be further increased once the primary reflection loss at the front side (caused by nonideal ETLs) could be reduced without the sacrifice of electrical performance. Yet, little attention has been paid in planar PSCs to

X. Luo, Dr. Y. Gao, P. Zhu, Q. Han, R. Lin, H. Gao, Y. Wang, Prof. J. Zhu, Prof. H. Tan
National Laboratory of Solid State Microstructures
Jiangsu Key Laboratory of Artificial Functional Materials
College of Engineering and Applied Sciences
Nanjing University
Nanjing 210093, China
E-mail: hairentan@nju.edu.cn

X. Luo, Prof. S. Li
School of Electronics Science and Engineering
Nanjing University
Nanjing 210093, China
E-mail: sli@nju.edu.cn

The ORCID identification number(s) for the author(s) of this article can be found under https://doi.org/10.1002/solr.202000169.

DOI: 10.1002/solr.202000169

design an ETL that can simultaneously reduce primary reflection losses and improve device electrical performance.

Here, we pursued an ETL structure that enables both enhanced light capturing and improved electrical performance in n-i-p structured planar PSCs. We devised an antireflective cascaded ETL using SnO_2/TiO_2–Cl bilayered NC films (**Figure 1**a). The bilayer structure leads to reduced nonradiative recombination, cascaded energy levels, and lower optical reflection losses. Based on this strategy, we achieved a record-high J_{sc} of 26.1 mA cm^{-2} and a PCE of 22.9% in $FAPbI_3$-based planar PSCs (optical bandgap of 1.54 eV), where the J_{sc} is comparable to those achieved in most-efficient mesoporous cells.

To compare the photovoltaic performance on different ETLs, we fabricated $FAPbI_3$-based planar PSCs on SnO_2 single-layer and SnO_2/TiO_2–Cl bilayer ETLs (Figure 1a). According to Fresnel equations, tuning the refractive index and thickness of ETLs (functioning as an antireflective structure as well) is crutial to minimize the primary optical reflection in planar PSCs. Constructing bilayer ETL structure, in principle, offers the potential to further lower the reflection over a broader spectral range compared with single-layer ETL. The perovskite absorber layers, with a composition of $FA_{0.92}MA_{0.08}PbI_3$, were fabricated by two-step sequential deposition according to previous works which have demonstrated record-efficiency planar PSCs.[5] The statistical performance from 28 devices for each ETL is shown in Figure 1b. Planar PSCs with SnO_2/TiO_2–Cl ETL exhibit considerably higher average PCE than those with SnO_2 ETL (21.9% vs 19.8%). The improvement comes mainly from J_{sc} and open-circuit voltage (V_{oc}), where the average J_{sc} increases from 24.5 to 25.3 mA cm^{-2} and V_{oc} increases from 1.06 to 1.12 V. We noted that the performance of cells with antireflective cascaded ETL was more reproducible than that of devices with SnO_2 ETL, as indicated by the narrower PCE distribution. We also observed less hysteresis in PSCs with the cascaded ETL (Figure 1c), which can be attributed to faster charge extraction and reduced interfacial trap density (which will be discussed later). The PSCs with SnO_2/TiO_2–Cl ETL exhibited better shelf stability than those with SnO_2 ETL (Figure S1, Supporting Information).

The best-performing cells with SnO_2 and SnO_2/TiO_2–Cl ETLs showed PCEs of 20.8% (stabilized 19.9%) and 22.3% (stabilized 21.7%) under reverse scans, respectively (Figure 1c, Figure S2, Supporting Information). The specific photovoltaic parameters

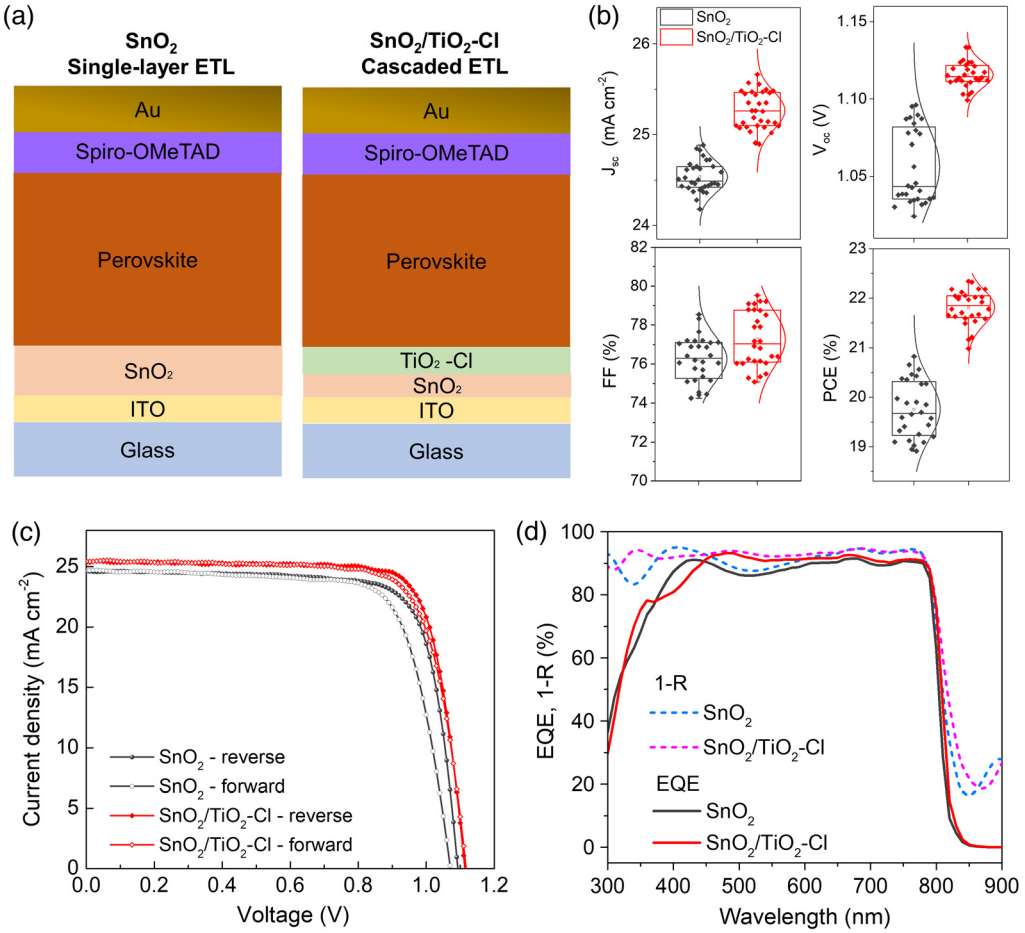

Figure 1. Photovoltaic performance of PSCs with antireflective cascaded ETL. a) Device structures of planar PSCs with SnO_2 and cascaded SnO_2/TiO_2–Cl ETLs. b) Comparison of photovoltaic parameters (J_{sc}, V_{oc}, FF, and PCE) for solar cells with SnO_2 and SnO_2/TiO_2–Cl ETLs. c) J–V curves of champion devices based on SnO_2 and SnO_2/TiO_2–Cl ETLs. d) $1-R$ (total absorptance of solar cell) and EQE spectra of the champion devices. The integrated J_{sc} values are 24.5 and 25.3 mA cm^{-2} for devices on SnO_2 and SnO_2/TiO_2–Cl ETLs, respectively.

Table 1. Photovoltaic parameters of champion planar PSCs with SnO_2 and SnO_2/TiO_2–Cl ETLs.

ETL	Scan direction	J_{sc} [mA cm^{-2}]	V_{oc} [V]	FF [%]	PCE [%]
SnO_2	Reverse	24.6	1.093	77.3	20.8
	Forward	24.7	1.071	74.5	19.7
SnO_2/TiO_2–Cl	Reverse	25.3	1.114	79.1	22.3
	Forward	25.4	1.117	76.2	21.6

are summarized in **Table 1**. Figure 1d shows the EQE and total absorptance ($1-R$, where R is device reflectance) curves of planar PSCs on SnO_2 and SnO_2/TiO_2–Cl ETLs. As observed in previous works,[5,23,24] the PSCs with SnO_2 ETL (thickness optimized to be ≈30 nm) exhibited an obvious dip in the EQE curves between 400–700 nm, due to a strong optical reflection peak in this wavelength range. By inserting another layer of TiO_2–Cl (≈60 nm) between SnO_2 and perovskite, the reflection loss is significantly reduced in devices with SnO_2/TiO_2–Cl ETL, leading to increased EQE values overall. The peak reflectance intensities of 17% between 300–400 nm and 12% between 400–600 nm in devices with SnO_2 ETL were reduced to 5% and 7%, respectively, in devices with SnO_2/TiO_2–Cl ETLs. The integrated J_{sc} from EQE spectra was increased from 24.5 to 25.3 mA cm^{-2}, which are in good agreement with those values measured from J–V scans. We further tested the cascaded ETL in PSCs with a perovskite composition of $(FAPbI_3)_{0.97}(MAPbBr_3)_{0.03}$, and similar performance enhancement by cascaded ETL was observed (Figure S3, Supporting Information). Unless otherwise stated, the perovskite composition studied in this work refers to $FA_{0.92}MA_{0.08}PbI_3$.

The improvement in J_{sc} by SnO_2/TiO_2–Cl ETL is attributed dominantly to the reduced primary reflection at the ETL/perovskite interface. To gain further insight into the improvement in electrical performance (mainly V_{oc} here), we first calculated the valence band (E_{VB}) and the conduction band (E_{CB}) of ETLs and perovskite layer using ultraviolet photoelectron spectroscopy (UPS) and UV–vis–NIR spectroscopy (**Figure 2**a and Figure S4, Supporting Information). The band alignment shows that the SnO_2/TiO_2–Cl bilayered ETL has cascaded conduction bands with the perovskite layer, which is beneficial for the electron extraction. The smaller band offset between TiO_2–Cl and perovskite than SnO_2 helps increase V_{oc} in solar cells. We further investigated the perovskite films deposited on SnO_2 and SnO_2/TiO_2–Cl ETLs using scanning electron microscopy (SEM) and X-ray diffraction (XRD). We found that the perovskite films grown on SnO_2/TiO_2–Cl ETL exhibited larger grain sizes and more uniform size distribution than those on SnO_2 (Figure S5, Supporting Information). Cross-sectional SEM images show that the perovskite layers (around 850 nm thick) had a columnar character for the crystal grains from the bottom to top. XRD patterns showed similar crystallinity and identical crystal structure for films grown on either ETL (Figure 2b).

We further characterized the carrier extraction characteristics between ETL and perovskite using steady-state photoluminescence (PL) and time-resolved PL decay (Figure 2c, d). We observed stronger PL quenching in intensity and faster PL decay for perovskite films on SnO_2/TiO_2–Cl than those on SnO_2, which indicates faster extraction of carriers at the cascaded ETL/perovskite interface. We then carried out space-charge-limited-current (SCLC) tests to quantitatively estimate the bulk trap density in perovskite films grown on SnO_2 and SnO_2/TiO_2–Cl ETLs using a device structure of glass/ITO/ETL/perovskite/C_{60}/BCP/Cu, where C_{60} is fullerene and BCP is bathocuproine (Figure 2e). The trap density N_t is calculated from the equation $V_{TFL} = \frac{eN_tL^2}{2\varepsilon\varepsilon_0}$,[36] where e is the elementary charge, L the thickness of perovskite film, ε the relative dielectric constant, ε_0 the vacuum permittivity, and V_{TFL} the trap-filling voltage. The trap densities are calculated to be 7.1×10^{15} and 3.4×10^{15} cm^{-3} for perovskite films grown on SnO_2 and SnO_2/TiO_2–Cl ETLs, respectively. A lower dark saturation-current density was also observed for PSCs with SnO_2/TiO_2–Cl ETL (Figure S6, Supporting Information), in agreement with the lower trap density for perovskite films grown on SnO_2/TiO_2–Cl. We proceeded to use transient photovoltage decay technique to characterize solar cells with SnO_2 and SnO_2/TiO_2–Cl ETLs. The charge-recombination lifetime τ of devices with SnO_2/TiO_2–Cl is longer than that of devices with SnO_2 (38 vs 12 μs). The longer recombination lifetime in devices with SnO_2/TiO_2–Cl ETL is attributed to the reduced recombination rates at the cascaded ETL/perovskite interface and lower bulk trap density in perovskite films grown on the cascaded ETL.[37]

To further understand the optical improvement by the cascaded ETL, we performed optical modeling of planar PSCs using a validated optical model (GenPro4).[38] We measured the complex refractive index of each layer using ellipsometry (Figure S7, Supporting Information). We calculated the optical reflection and implied photocurrent density (integration of the absorption by the perovskite layer with AM 1.5G spectrum) by varying the thickness of SnO_2 and TiO_2–Cl layers (**Figure 3**a). The thicknesses of other layers were fixed and derived from experimental measurements. As expected from thin-film optics, the device primary reflectance and thus the implied J_{sc} values are dependent on the thickness of ETL. If only optical absorption was considered, the highest J_{sc} could be achieved with SnO_2 single layer at a thickness of ≈110 nm.

In addition to the optical effect, the electrical properties of the ETL, i.e., conductivity and charge extraction capability, play a crucial role in the performance of solar cells. We characterized the vertical electrical resistance of ETLs with various thicknesses and stacking sequences using a sandwiched structure of ITO/ETL/Al (Figure 3b). The resistance of single-layer SnO_2 is higher than that of TiO_2–Cl for each thickness (30, 60, and 90 nm), indicating a better conductivity for TiO_2–Cl NC film. It is interesting to note that the cascaded ETL stack (30 nm SnO_2 + 60 nm TiO_2–Cl) has a lower resistance than that of either 30 nm SnO_2 or 60 nm TiO_2–Cl film. This offers benefit of increasing J_{sc} (as indicated by the optical simulation shown in Figure 3a) without increasing the resistance of ETL when thicker ETL layer stack is used. In contrast, reversing the ETL stack to TiO_2-Cl/SnO_2 led to a Schottky-diode-like behavior and thus resulted in significantly higher resistance, which could be induced by the Schottky barrier (≈0.2 eV) for electron transporting from SnO_2 to TiO_2–Cl.

We then fabricated PSCs with varied ETLs and characterized their photovoltaic performance (Figure 3c and S8, Table S1, Supporting Information). Unlike the simulation results, the J_{sc}

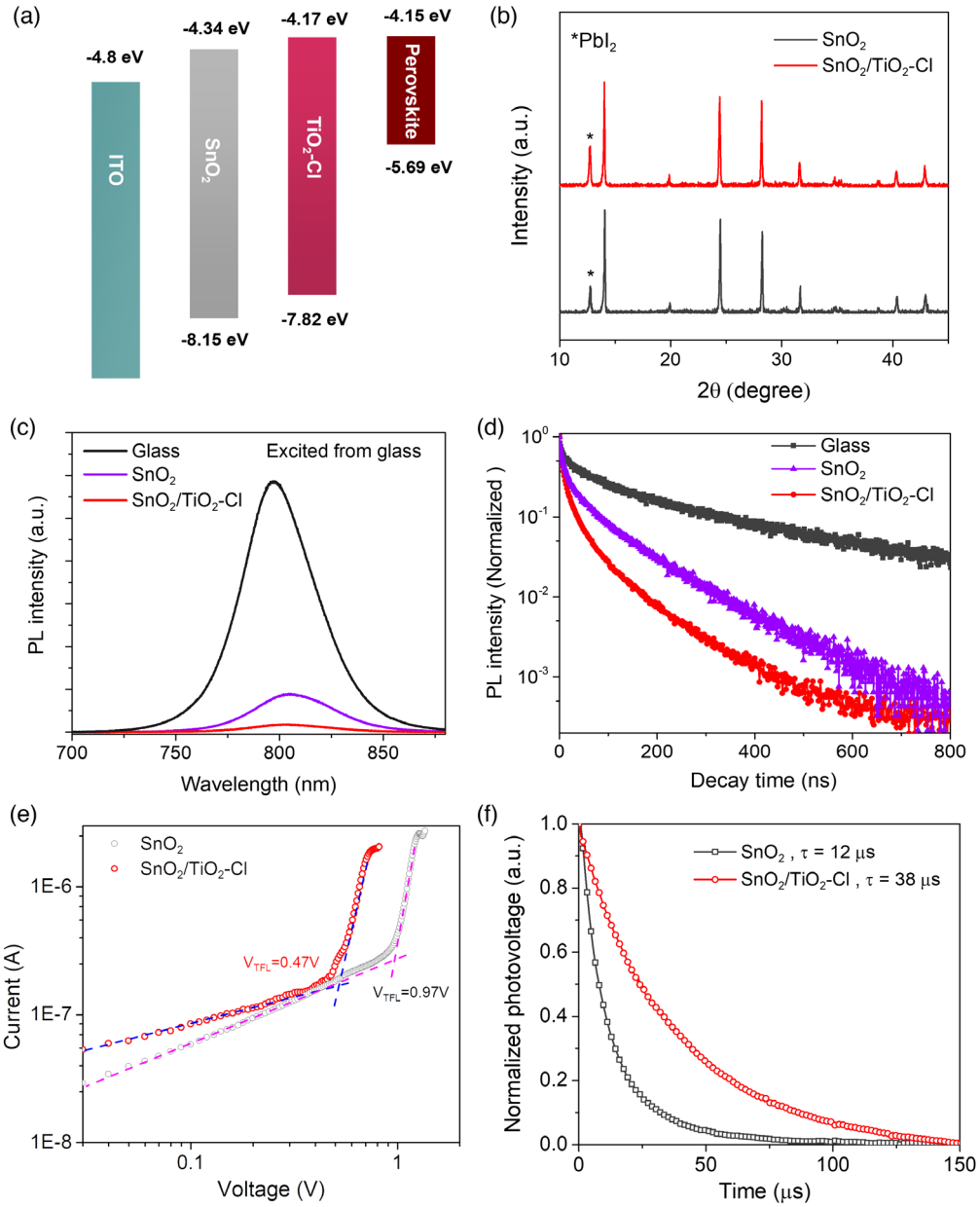

Figure 2. Characterization of perovskite films deposited on SnO_2 and SnO_2/TiO_2–Cl ETLs. a) Band alignment of SnO_2, TiO_2–Cl, and perovskite layer. b) XRD patterns of perovskite films deposited on SnO_2 and SnO_2/TiO_2–Cl ETLs. c,d) Steady-state and time-resolved PL spectra of perovskite films on glass, SnO_2 and SnO_2/TiO_2–Cl ETLs excited from glass side. e) SCLC measurements of electron-only devices with SnO_2 and SnO_2/TiO_2–Cl ETLs. f) Transient photovoltage measurements of solar cells based on SnO_2 and SnO_2/TiO_2–Cl ETLs.

of solar cells with SnO_2 ETL did not increase as the thickness of SnO_2 increased from 30 to 90 nm. Instead, the average V_{oc} dropped significantly as the thickness of SnO_2 ETL was increased; the J_{sc} started to decrease when the thickness of SnO_2 increased beyond 40 nm. In contrast, the performance of devices with TiO_2–Cl ETL is less sensitive to the thickness of TiO_2–Cl and the average V_{oc} and fill factor (FF) did not obviously change as the thickness increased from 30 to 90 nm, which can be explained by the higher conductivity of TiO_2–Cl film in comparison to SnO_2. The optimized thicknesses of single-layer ETLs are 30 and 60 nm for SnO_2 and TiO_2–Cl ETLs, respectively. We then evaluated the performance of PSCs with SnO_2/TiO_2–Cl cascaded ETL, where the SnO_2 layer was fixed at 30 nm and the TiO_2–Cl layer was varied from 30 to 90 nm. The highest average PCE was achieved with a total thickness of 90 nm for the cascaded ETL. Further increasing its thickness to 120 nm caused partial delamination of perovskite films from the substrates, leading to an obvious drop in J_{sc} and V_{oc}. Herein, we can conclude that the series resistance of the ETL is a determining factor for the cell performance. It should be also noted that the ETL stack sequence is

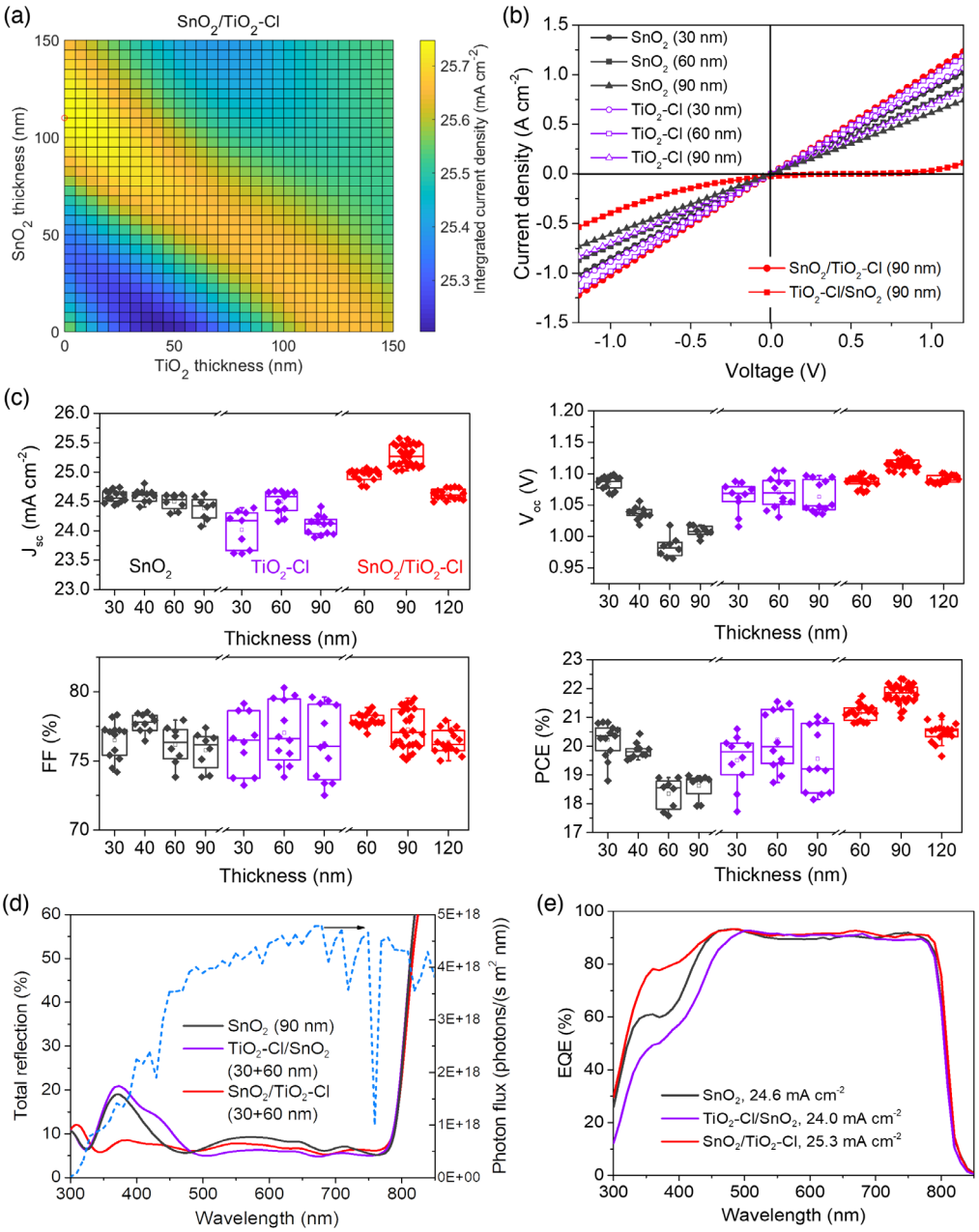

Figure 3. Photovoltaic performance of PSCs with varied thicknesses of ETL. a) Calculated implied J_{sc} of solar cells by varying the thickness of SnO_2 and TiO_2–Cl layers in the cascaded ETL stack. b) Dark *J–V* characteristics of ITO/ETL/Al structures with various thickness and stacking sequence of ETL. c) Photovoltaic parameters (V_{oc}, J_{sc}, FF, and PCE) of solar cells with various thicknesses of SnO_2, TiO_2, and SnO_2/TiO_2–Cl ETLs. The thickness of SnO_2 layer in SnO_2/TiO_2–Cl ETLs (total thickness shown in the figure) was fixed at 30 nm. d) Device total reflectance curves (left) of PSCs based on SnO_2 (90 nm), TiO_2–Cl/SnO_2 (60 + 30 nm), and SnO_2/TiO_2–Cl (30 + 60 nm) ETLs, and the photon flux of the global standard spectrum AM1.5 G (right). e) EQE curves of PSCs SnO_2 (90 nm), TiO_2-Cl/SnO_2 (60 + 30 nm), and SnO_2/TiO_2–Cl (30 + 60 nm) ETLs.

crucial to the performance of solar cells. Reversing the stack sequence to TiO_2–Cl/SnO_2 led to poor photovoltaic performance due to its Schottky-barrier characteristics, though low primary reflectance at the front side could be achieved in the visible-spectral range (Figure 3d,e and S4d, Supporting Information).

To further reduce the optical reflection loss at the front glass surface, we attached a nanostructured antireflective foil (ARF) on the front glass side (**Figure 4**a).[39] As a result, the overall primary reflectance was reduced by ≈3% between 300 and 800 nm wavelength range, resulting in an obvious increase in EQE (Figure 4b). The PCE of the identical device was improved from 22.3% to 22.8% after the deployment of ARF (Figure 4c and **Table 2**). The J_{sc} values can be reproducibly increased by ≈0.6 mA cm^{-2} after adding an antireflective coating at the front

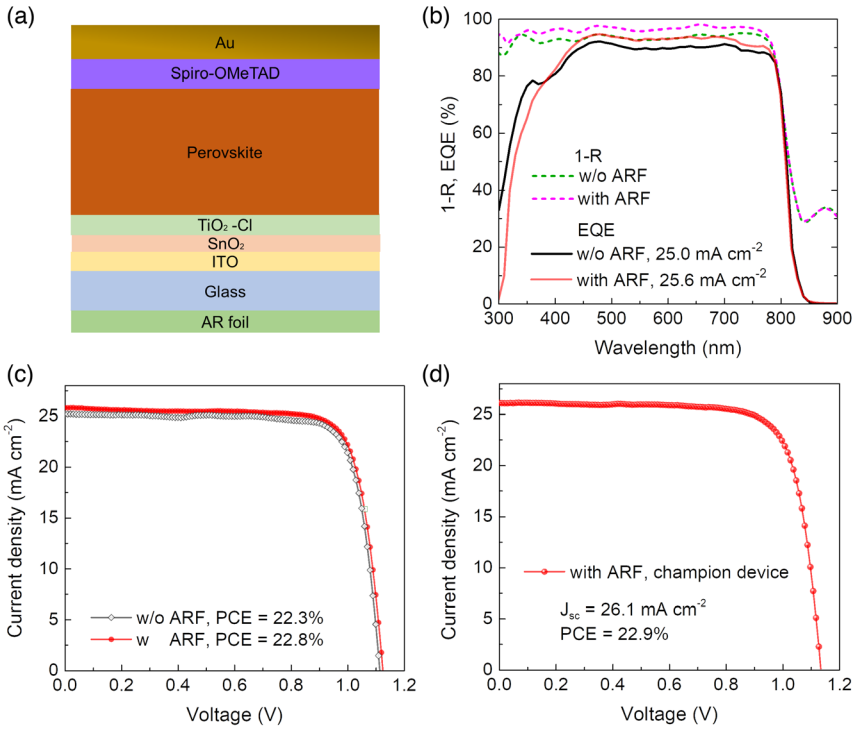

Figure 4. Performance enhancement of PSCs using antireflective foil at the front of glass surface. a) Structure of PSC with cascaded ETL and ARF. b) $1-R$ and EQE curves of a PSC without and with ARF. c) J–V curves of the device with and without AR film under reverse scans. d) J–V curve of the champion device with ARF under reverse scan.

Table 2. Photovoltaic parameters of PSCs with and without ARF.

Device	J_{sc} [mA cm^{-2}]	V_{oc} [V]	FF [%]	PCE [%]
w/o ARF	25.2	1.114	79.3	22.3
with ARF	25.8	1.125	78.7	22.8
Champion (with ARF)	26.1	1.137	77.1	22.9

side of glass substrate (Figure S9 and Table S2, Supporting Information), despite of the parasitic absorption loss of ARF itself below 400 nm wavelengths (Figure S10a, Supporting Information). By fabricating several batches of planar PSCs with both cascaded ETL and ARF, we obtained the best PCE of 22.9%, with a V_{oc} of 1.137 V, J_{sc} of 26.1 mA cm^{-2}, and FF of 77.1% (Figure 4d). The integrated J_{sc} value from the EQE spectra is 25.7 mA cm^{-2} (Figure S10b, Supporting Information), in good agreement with the J–V measurements.

In summary, we have devised an antireflective cascaded SnO_2/TiO_2–Cl ETL that can effectively increase the photocurrent density of planar PSC without compromising in electrical performance. The primary optical reflection of planar PSCs at the front side can be dramatically reduced using cascaded ETL. Based on this strategy, we achieved a record-high J_{sc} of 26.1 mA cm^{-2} and a high PCE of 22.9% in $FAPbI_3$-based planar PSCs. The J_{sc} values achieved herein are comparable to those achieved in most-efficient mesoporous PSCs reported so far. The proposed antireflective cascaded ETL strategy offers a simple and versatile approach to improve the efficiency of planar PSCs.

Supporting Information

Supporting Information is available from the Wiley Online Library or from the author.

Acknowledgements

X.L. and Y.G. contributed equally to this work. This work was financially supported by the National Key R&D Program of China (2018YFB1500102), the National Natural Science Foundation of China (61974063), Natural Science Foundation of Jiangsu Province (BK20190315, BZ2018008), the Thousand Talent Program for Young Outstanding Scientists in China, and Program for Innovative Talents and Entrepreneur in Jiangsu. The authors thank Dr. Hitoshi Sai from AIST (Japan) for providing the ARF used in this work.

Conflict of Interest

The authors declare no conflict of interest.

Keywords

antireflections, cascaded electron transport layers, planar perovskite solar cells, short-circuit current density

Received: March 30, 2020
Published online: April 23, 2020

[1] A. Kojima, K. Teshima, Y. Shirai, T. Miyasaka, *J. Am. Chem. Soc.* **2009**, *131*, 6050.
[2] M. M. Lee, J. Teuscher, T. Miyasaka, T. N. Murakami, H. J. Snaith, *Science* **2012**, *338*, 643.
[3] M. Grätzel, *Nat. Mater.* **2014**, *13*, 838.
[4] Best Research-Cell Efficiency Chart, https://www.nrel.gov/pv/cell-efficiency.html (accessed: March 2020).
[5] Q. Jiang, Y. Zhao, X. Zhang, X. Yang, Y. Chen, Z. Chu, Q. Ye, X. Li, Z. Yin, J. You, *Nat. Photonics* **2019**, *13*, 460.
[6] H. Min, M. Kim, S. U. Lee, H. Kim, G. Kim, K. Choi, J. H. Lee, S. Il Seok, *Science* **2019**, *366*, 749.
[7] R. Lin, K. Xiao, Z. Qin, Q. Han, C. Zhang, M. Wei, M. I. Saidaminov, Y. Gao, J. Xu, M. Xiao, A. Li, J. Zhu, E. H. Sargent, H. Tan, *Nat. Energy* **2019**, *4*, 864.
[8] F. Giordano, A. Abate, J. P. Correa Baena, M. Saliba, T. Matsui, S. H. Im, S. M. Zakeeruddin, M. K. Nazeeruddin, A. Hagfeldt, M. Graetzel, *Nat. Commun.* **2016**, *7*, 10379.
[9] Y. Rong, L. Liu, A. Mei, X. Li, H. Han, *Adv. Energy Mater.* **2015**, *5*, 1501066.
[10] J. J. Choi, X. Yang, Z. M. Norman, S. J. L. Billinge, J. S. Owen, *Nano Lett.* **2014**, *14*, 127.
[11] H.-S. Kim, N.-G. Park, *J. Phys. Chem. Lett.* **2014**, *5*, 2927.
[12] D. Yang, R. Yang, K. Wang, C. Wu, X. Zhu, J. Feng, X. Ren, G. Fang, S. Priya, S. (Frank) Liu, *Nat. Commun.* **2018**, *9*, 3239.
[13] G. Yang, H. Lei, H. Tao, X. Zheng, J. Ma, Q. Liu, W. Ke, Z. Chen, L. Xiong, P. Qin, Z. Chen, M. Qin, X. Lu, Y. Yan, G. Fang, *Small* **2017**, *13*, 1601769.
[14] Q. Jiang, L. Zhang, H. Wang, X. Yang, J. Meng, H. Liu, Z. Yin, J. Wu, X. Zhang, J. You, *Nat. Energy* **2017**, *2*, 1.
[15] D. Liu, T. L. Kelly, *Nat. Photonics* **2014**, *8*, 133.
[16] W. R. Erwin, H. F. Zarick, E. M. Talbert, R. Bardhan, *Energy Environ. Sci.* **2016**, *9*, 1577.
[17] Y. Yamada, T. Nakamura, M. Endo, A. Wakamiya, Y. Kanemitsu, *IEEE J. Photovoltaics* **2015**, *5*, 401.
[18] Y. Yamada, T. Nakamura, M. Endo, A. Wakamiya, Y. Kanemitsu, *Appl. Phys. Express* **2014**, *7*, 032302.
[19] W. S. Yang, B. W. Park, E. H. Jung, N. J. Jeon, Y. C. Kim, D. U. Lee, S. S. Shin, J. Seo, E. K. Kim, J. H. Noh, S. Il Seok, *Science* **2017**, *356*, 1376.
[20] Y. Liu, S. Akin, L. Pan, R. Uchida, N. Arora, J. V. Milić, A. Hinderhofer, F. Schreiber, A. R. Uhl, S. M. Zakeeruddin, A. Hagfeldt, M. I. Dar, M. Grätzel, *Sci. Adv.* **2019**, *5*, eaaw2543.
[21] M. Kim, G. H. Kim, T. K. Lee, I. W. Choi, H. W. Choi, Y. Jo, Y. J. Yoon, J. W. Kim, J. Lee, D. Huh, H. Lee, S. K. Kwak, J. Y. Kim, D. S. Kim, *Joule* **2019**, *3*, 2179.
[22] M. A. Green, Y. Hishikawa, E. D. Dunlop, D. H. Levi, J. Hohl-Ebinger, M. Yoshita, A. W. Y. Ho-Baillie, *Prog. Photovoltaics Res. Appl.* **2019**, *27*, 3.
[23] Q. Jiang, L. Zhang, H. Wang, X. Yang, J. Meng, H. Liu, Z. Yin, J. Wu, X. Zhang, J. You, *Nat. Energy* **2017**, *2*, 16177.
[24] P. Zhu, S. Gu, X. Luo, Y. Gao, S. Li, J. Zhu, H. Tan, *Adv. Energy Mater.* **2020**, *10*, 1903083.
[25] Y. Zhao, H. Tan, H. Yuan, Z. Yang, J. Z. Fan, J. Kim, O. Voznyy, X. Gong, L. N. Quan, C. S. Tan, J. Hofkens, D. Yu, Q. Zhao, E. H. Sargent, *Nat. Commun.* **2018**, *9*, 1.
[26] G. Yang, C. Chen, F. Yao, Z. Chen, Q. Zhang, X. Zheng, J. Ma, H. Lei, P. Qin, L. Xiong, W. Ke, G. Li, Y. Yan, G. Fang, *Adv. Mater.* **2018**, *30*, 1706023.
[27] N. Li, S. Tao, Y. Chen, X. Niu, C. K. Onwudinanti, C. Hu, Z. Qiu, Z. Xu, G. Zheng, L. Wang, Y. Zhang, L. Li, H. Liu, Y. Lun, J. Hong, X. Wang, Y. Liu, H. Xie, Y. Gao, Y. Bai, S. Yang, G. Brocks, Q. Chen, H. Zhou, *Nat. Energy* **2019**, *4*, 408.
[28] J. Wu, Y. Cui, B. Yu, K. Liu, Y. Li, H. Li, J. Shi, H. Wu, Y. Luo, D. Li, Q. Meng, *Adv. Funct. Mater.* **2019**, *29*, 1905336.
[29] M. Jošt, S. Albrecht, L. Kegelmann, C. M. Wolff, F. Lang, B. Lipovšek, J. Krč, L. Korte, D. Neher, B. Rech, M. Topič, *ACS Photonics* **2017**, *4*, 1232.
[30] B. Shi, B. Liu, J. Luo, Y. Li, C. Zheng, X. Yao, L. Fan, J. Liang, Y. Ding, C. Wei, D. Zhang, Y. Zhao, X. Zhang, *Sol. Energy Mater. Sol. Cells* **2017**, *168*, 214.
[31] A. R. Pascoe, S. Meyer, W. Huang, W. Li, I. Benesperi, N. W. Duffy, L. Spiccia, U. Bach, Y. B. Cheng, *Adv. Funct. Mater.* **2016**, *26*, 1278.
[32] W. Zhang, Y. Jiang, Y. Ding, M. Zheng, S. Wu, X. Lu, X. Gao, Q. Wang, G. Zhou, J. Liu, M. J. Naughton, K. Kempa, J. Gao, *Opt. Mater. Express* **2017**, *7*, 2150.
[33] F. Huang, A. R. Pascoe, W. Q. Wu, Z. Ku, Y. Peng, J. Zhong, R. A. Caruso, Y. B. Cheng, *Adv. Mater.* **2017**, *29*, 1601715.
[34] Y. Zhong, R. Munir, A. H. Balawi, A. D. Sheikh, L. Yu, M. C. Tang, H. Hu, F. Laquai, A. Amassian, *ACS Energy Lett.* **2016**, *1*, 1049.
[35] C. Y. Xu, W. Hu, G. Wang, L. Niu, A. M. Elseman, L. Liao, Y. Yao, G. Xu, L. Luo, D. Liu, G. Zhou, P. Li, Q. Song, *ACS Nano* **2020**, *14*, 196.
[36] D. Shi, V. Adinolfi, R. Comin, M. Yuan, E. Alarousu, A. Buin, Y. Chen, S. Hoogland, A. Rothenberger, K. Katsiev, Y. Losovyj, X. Zhang, P. A. Dowben, O. F. Mohammed, E. H. Sargent, O. M. Bakr, *Science* **2015**, *347*, 519.
[37] H. Tan, A. Jain, O. Voznyy, X. Lan, F. P. G. De Arquer, J. Z. Fan, R. Quintero-Bermudez, M. Yuan, B. Zhang, Y. Zhao, F. Fan, P. Li, L. N. Quan, Y. Zhao, Z. H. Lu, Z. Yang, S. Hoogland, E. H. Sargent, *Science* **2017**, *355*, 722.
[38] R. Santbergen, T. Meguro, T. Suezaki, G. Koizumi, K. Yamamoto, M. Zeman, *IEEE J. Photovoltaics* **2017**, *7*, 919.
[39] H. Sai, T. Matsui, K. Saito, M. Kondo, I. Yoshida, *Prog. Photovoltaics Res. Appl.* **2015**, *23*, 1572.